Design methodology for graphene tunable filters at the sub–millimeter–wave frequencies

Ilić, A.Z., Bukvić, B.M., Budimir, D. and Ilić, M.M.

Design methodology for graphene tunable filters at the sub–millimeter–wave frequencies

Andjelija Ž. Ilić, Branko M. Bukvić, Djuradj Budimir, Milan M. Ilić

PII: S0038-1101(18)30590-2
DOI: https://doi.org/10.1016/j.sse.2019.04.003
Reference: SSE 7602

To appear in: *Solid-State Electronics*

Received Date: 14 October 2018
Revised Date: 24 February 2019
Accepted Date: 28 April 2019

Please cite this article as: Ilić, A.Z., Bukvić, B.M., Budimir, D., Ilić, M.M., Design methodology for graphene tunable filters at the sub–millimeter–wave frequencies, *Solid-State Electronics* (2019), doi: https://doi.org/10.1016/j.sse.2019.04.003

Title:

Design methodology for graphene tunable filters at the sub-millimeter-wave frequencies

Authors:

Andjelija Ž. Ilić[a,*], Branko M. Bukvić[b], Djuradj Budimir[c,d], and Milan M. Ilić[d,e]

(Family names: Ilić, Bukvić, Budimir, Ilić)

(Email addresses: andjelijailic@ieee.org , bukvic.branko@gmail.com , d.budimir@westminster.ac.uk , milanilic@etf.bg.ac.rs)

Affiliations:

[a] Institute of Physics Belgrade, Pregrevica 118, 11080 Zemun-Belgrade, Serbia

[b] IMTEL-communication, Bulevar Mihajla Pupina 165b, 11070 Belgrade, Serbia

[c] Wireless Communications Research Group, University of Westminster, London W1W 6UW, UK

[d] School of Electrical Engineering, University of Belgrade, 11120 Belgrade, Serbia

[e] ECE Department, Colorado State University, Fort Collins, CO 80523-1373, USA

* Corresponding author: Andjelija Ž. Ilić, phone: +381 11 6157577, fax: +381 11 3248681
andjelijailic@ieee.org

Abstract:

Tunable components and circuits, allowing for the fast switching between the states of operation, are among the basic building blocks for future communications and other emerging applications. Based on the previous thorough study of graphene based resonators, the design methodology for graphene tunable filters has been devised, outlined, as well as explained through an example of the fifth order filter. The desired filtering responses can be achieved with the material loss not higher than the loss corresponding to the previously studied single resonators, depending mostly on the quantity of graphene per resonator. The proposed design method relies on the detailed design space mapping; obtained data gives an immediate assessment of the feasibility of specifications with a particular filter order, maximal passband ripple level, desired bandwidth, and acceptable losses. The design process could be further automated by the knowledge based approach using the collected design space data.

Keywords: Tunable bandpass filters (BPF), graphene, sub-millimeter wave filters, full-wave numerical model, equivalent circuit, design method

Declarations of interest: None.

Role of funding source: No funding body had any involvement in the preparation or content of this article or in the decision to submit it for publication.

Design methodology for graphene tunable filters at the sub-millimeter-wave frequencies

1. Introduction

Advances and promises in the development of the terahertz power sources over the last two decades [1]–[3], as well as emerging commercial applications, have led to the increased efforts in the development of circuits and systems for use at the sub-millimeter wave (low-terahertz) frequencies. Components, including antennas [4]–[6], waveguides [6]–[8], filters [9], [10], diodes and transistors [11]–[13], and photonic devices [14]–[16], are being customized for use in this spectral region. Schottky diodes, used in mixers, multipliers, phase shifters, and detectors, have to be designed using approaches aimed at reducing the capacitances, in efforts to extend the frequencies of operation up to 1.5 THz [11]. Likewise, graphene-channel field-effect transistors are being developed, which can, with a careful design, help increase the cutoff frequencies to the terahertz range [12]. As the future broadband low-terahertz communications envision combined use of the optical and wireless technology [17], [18], it is of interest to develop mutually compatible devices and systems. Compact analog bandpass and bandstop filters are required as important basic building blocks of the high frequency systems [9], [19], [20]. Utilization of micromachining [7], [10], metamaterials [21], or new materials [5], [9], [14], is often needed to meet the design specifications. It is also highly desirable to reduce the circuit size by enabling the frequency-tunable or reconfigurable multiband operation of components. Although there are purely metallic sub-millimeter wave filters, the development of advanced tunable and reconfigurable solutions, such as the ones based on the utilization of novel materials [9], is highly important. Not only is the span of the available components broadened, but additionally, the theoretic basis for the utilization of similar concepts in a somewhat different setting is developed. Having that in mind, we have recently proposed and analyzed in detail graphene based tunable rectangular waveguide resonators [22]. Graphene has been proven as a very good material for sub-millimeter wave (low-terahertz) applications. In addition to the use in a design of frequency tunable circuits [5], [14], [16], [21]–[24], or other tunable properties [25], it exhibits excellent mechanical and structural properties, suitable for the design of flexible electronic circuits [25]–[27]. Theoretical expressions derived in [22], describing the influence of the variable surface conductivity on the electromagnetic (EM) field boundary conditions, could also be used to describe the future materials of possibly superior characteristics that are yet to be developed [21], [28], [29]. Here we consider the waveguide bandpass filters; however, the proposed methods, with modifications, could be easily applied to different structures, such as the surface integrated waveguide (SIW) or the planar printed circuits technology. Utilizing the resonators we proposed in [22], we suggest a design method relying on the detailed design space mapping, with a special emphasis on choosing the appropriate design parameters given the increased number of the degrees of freedom in a design. It is our main aim to define general procedures for

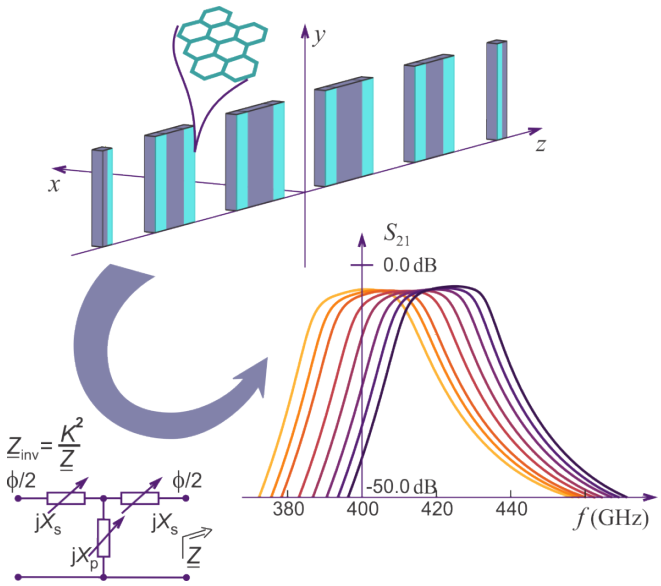

Fig. 1. Structure and operating principle of the graphene tunable filters utilizing *E*-plane discontinuities. In our design, graphene stripes are located along the inner edges of the *E*-plane inserts, next to the resonators, except at the ends of the structure where no resonators are formed and metallic edges are preferred for the best stopband attenuation (top figure). Variable surface conductivity of graphene, controlled via the electrostatic bias voltage, causes changes of the EM field distribution along the insert edges, influencing impedances of the normalized dominant mode equivalent circuit (bottom left). Effects are similar to varying the effective lengths of resonators, which results in the tunability of filter center frequency (bottom right).

TABLE I
THE OBTAINED FILTER DIMENSIONS FOR THE FIFTH ORDER FILTER

STANDARD WR-2.2 WAVEGUIDE SECTION		QUARTZ THICKNESS
a (μm)	b (μm)	d (μm)
559.0	279.5	35.0
WAVEGUIDE DISCONTINUITIES (μm, μm)		
(l_{M1}, l_{G1}) - outer	(l_{M2}, l_{G2}) - second	(l_{M3}, l_{G3}) - innermost
(30.0, 30.0)	(120.0, 70.0)	(170.0, 70.0)
WAVEGUIDE RESONATORS		
l_{rez1} (μm)	l_{rez2} (μm)	l_{rez3} (μm)
280.0	272.0	272.0

the design of this type of filters to meet the specifications with a small number of iterative adjustments.

The combined graphene-metal waveguide resonators, proposed in [22], exploit the possibility of attaining resonant frequency tunability by varying the surface conductivity of the graphene covered *E*-plane waveguide inserts. Dependence of the resonator properties on key design parameters, throughout the frequency range of interest (100 GHz–1100 GHz), has been studied in detail in [22]. The important issues to be addressed during a filter design include getting the most benefits out of the controllable material properties as well as adopting a systematic design approach to achieve the desired frequency tunability while meeting the planned filtering requirements in a relatively small number of steps. The design procedure is illustrated by a carbon based filter design example at 400 GHz. Apart from the already mentioned applications in emerging low-terahertz communications, as well as non-invasive imaging and spectroscopy, frequency range from 325 to 500 GHz is extensively used in radio astronomy. Due to the increased sensitivity requirements, the required instrumentation is often custom built. Tunable bandpass filters are of interest when one requires wideband operation in combination with increased sensitivity and high-speed processing [30], [31]. In hybrid and digital instrumentation, analog filters are used at reception to perform anti-aliasing.

Basic principle of operation of graphene tunable filters is illustrated in Fig. 1, where an example designed fifth order filter is drawn to scale and the corresponding frequency-tunable dominant mode equivalent circuit of a single resonator is shown. Ladder networks consisting of series and parallel reactances, as in the above equivalent circuit, are conveniently represented using the so-called *K*-inverters with the equivalent gain *K*, and the equivalent electrical length at ports, ϕ. The latter modifies the effective resonator length. In that way, the surface conductivity variation results in tunable dominant mode equivalent circuit reactances, which directly translates into the changes in the effective electrical lengths at ports connected to the resonators. Increase in the resonator electrical length results in its central frequency shift toward the lower frequencies and vice versa. The optimized filter dimensions for the filter shown in Fig. 1 are listed in Table 1. The obtained frequency response for a designed example is shown in Fig. 1, on the right. The influence of the tunable graphene surface conductivity to the boundary conditions in graphene covered discontinuity edges has been explained in detail in [22]. Enhanced graphene absorptance in the low-terahertz range, as a consequence of graphene layers being many times thinner than the skin depth of metals in this frequency range, has been demonstrated and theoretically explained in [32], [33], along with the analysis of transmittance, reflectance and the corresponding boundary conditions. High absorption ability of graphene is important for attaining tunability; on the other hand, it increases the insertion loss of the filter. Careful adjustment of parameters is required in order to meet the desired filtering response.

2. Influence of the graphene tunable surface conductivity on the *E*-plane waveguide discontinuities

The surface conductivity of graphene can be calculated using the Kubo formalism of statistical physics [34], [35]. In the millimeter and submillimeter wave frequency range, when spatial-dispersion effects are negligible, and also without the magnetic field bias, the Kubo formula reduces to

$$\sigma(\omega,\mu_c,\Gamma,T)=\frac{-\mathrm{j}q_e^2k_BT}{\pi\hbar^2(\omega-\mathrm{j}2\Gamma)}\left(\frac{\mu_c}{k_BT}+2\ln\left(e^{-\frac{\mu_c}{k_BT}}+1\right)\right). \quad (1)$$

In this case, surface conductivity results from the intraband contributions [36], [37], as opposed to the higher terahertz frequencies where the interband contributions are dominant and

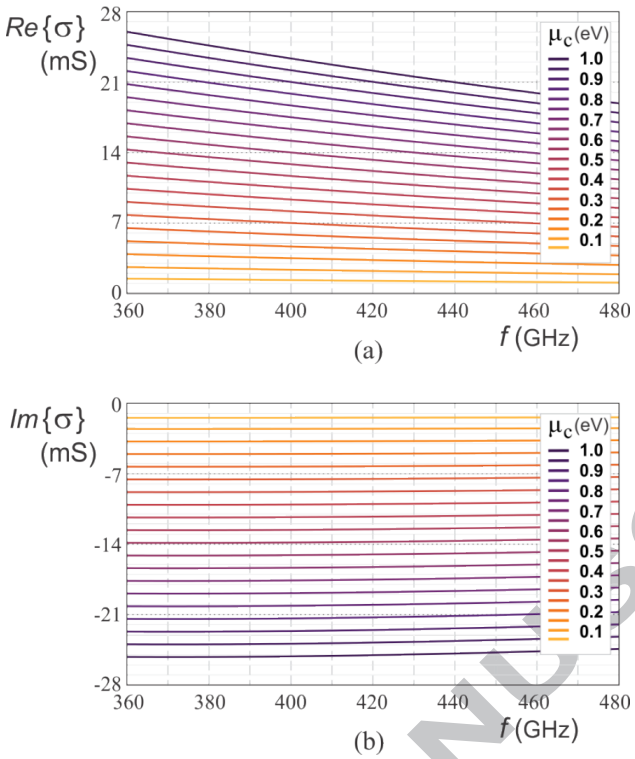

Fig. 2. Complex surface conductivity of graphene presented as the (a) real part and (b) imaginary part. Inverse of the surface conductivity, $Z_g=R_g+j\omega L_g$, required to set the boundary conditions for numerical EM computations, consists of a constant resistive part, R_g, and a reactance that depends linearly on frequency, $X_g=\omega L_g$.

the changes of surface conductivity with the applied bias field are more pronounced. Room temperature, $T=300$ K, is assumed. Elementary charge, Boltzmann constant, and the reduced Planck constant are denoted as q_e, k_B, and $\hbar$, respectively ($k_B=8.6173\times10^{-5}$ eV/K, $\hbar=1.0546\times10^{-34}$ Js.) The chemical potential, μ_c, k_BT product, and carrier scattering rate, Γ, are typically expressed in electronvolts. In (1), Γ is converted to s^{-1}. It is chosen to correspond to the high-quality multiple-graphene-layer sheets [38], with the relaxation time of charge carriers $\tau=(2\Gamma)^{-1}=3$ ps, desirable for a considered type of waveguide resonators [22]. The Fermi velocity in graphene is $v_F\approx10^6\frac{\text{m}}{\text{s}}$. The angular frequency of the external electromagnetic field is denoted by ω. The changes of conductivity with μ_c, in the considered frequency range, are presented in Fig. 2. Unlike the predominantly real graphene conductivity below 100 GHz, which also exhibits small variation with frequency, in the low-terahertz range it is inductive and adjustable by varying μ_c. The conductivity and shielding effects of graphene are modified by using the electrostatic bias field, E_{bias}, perpendicular to the graphene surface, which in addition to the chemical doping induces electrostatic doping, changing μ_c [37]:

$$\frac{\varepsilon_0\pi\hbar^2v_F^2}{q_e}E_{bias}=\int_0^{+\infty}\vartheta\left[(1+e^{(\vartheta-\mu_c)/k_BT})^{-1}-(1+e^{(\vartheta+\mu_c)/k_BT})^{-1}\right]d\vartheta\,. \quad (2)$$

Bias field can be realized through very thin slits in the waveguide wall next to the *E*-plane inserts, where the high frequency EM field components vanish. Bias field results from the bias voltage across the capacitor formed by graphene layers on both sides of a thin dielectric. Such configuration avoids a metallic gating electrode [39], [40], which would mask the effects of graphene conductivity. The dielectric layer is taken here as a 100 nm thick Al_2O_3. The described graphene stack is electrically very thin, thus the boundary conditions are assumed constant along its width and the effect of the very small slits used for biasing is considered negligible to the EM field distribution. To allow for the easier interpretation of results, surface conductivity is described in terms of the resulting chemical potential, rather than the applied bias voltage.

High-quality graphene layers can be obtained by using the mechanical exfoliation of graphite or growth on the epitaxial SiC. In contrast to some other graphene applications, such as high-frequency absorbers, where an excellent response has also been obtained in the case of CVD graphene regardless of the graphene grain size [41], [42], lower quality graphene might not be appropriate for the *E*-plane filter design. Namely, if the insertion loss were to increase, the filtering characteristics would deteriorate and the implementation of such filter could become impractical. To obtain the most accurate conductivity data, it is best to perform a detailed material characterization, since parameter values depend on manufacturing processes.

Various approaches have been reported in the literature for realizing tunable device properties. In [5], two modes of operation for the graphene patches were the low resistance mode (bias voltage applied), and the high resistance mode (no bias). By turning

different combinations of patches in a MIMO array on and off, a reconfigurable antenna radiation pattern is obtained. Number of reconfiguration states, as well as the beamwidth, is controlled by increasing the number of array elements. In [25], graphene is used for its flexibility and robustness in combination with the PDMS pyramid dielectric layers in realization of tunable capacitance pressure sensor. In [14], the varying surface conductivity of graphene has been employed to modulate the transmission between nearly zero and unity over a broad range of carrier frequencies up to a few THz. In [32], [33], polarization sensitivity of the transmittance and reflectance of graphene layers is used in tuning the polarization state of the transmitted and reflected wave. It can be controlled via changes to the surface conductivity, number of graphene layers and/or angle of incidence. In [43], graphene has been used in combination with the epsilon-near-zero (ENZ) metamaterial, where ENZ material contributes to the almost perfect EM absorption in the graphene layers. Here, the changes in graphene surface conductivity modify the effective length of the resonators, causing a shift of the filter center frequency. The surface impedance of graphene, $Z_g=R_g+j\omega L_g$, obtained as the inverse of (1), can be expressed as

$$R_g = 2\Gamma \frac{q_e}{\hbar} L_g \,, \tag{3}$$

$$L_g = \frac{\pi\hbar^2}{q_e^3 k_B T}\left(\frac{\mu_c}{k_B T}+2\ln(e^{-\mu_c/(k_B T)}+1)\right)^{-1} . \tag{4}$$

The structure of the proposed carbon based filters is shown in the top part of Fig. 1. In case of the combined graphene-metal waveguide resonators, only the edges of each *E*-plane insert consist of graphene sheets, i.e. vertical stripes. The rest of the inserts in between these stripes consist of a thin layer metallization. Both graphene and metallization are assumed to be supported by fused silica quartz holders. It is a material highly compatible with graphene, and also an excellent choice for the millimeter and submillimeter wave structures due to the relatively low dielectric constant and a small loss tangent.

Reasonable adhesion of metallic thin films, copper (Cu) or gold (Au), on quartz, can be achieved upon the pre-plating with a strongly oxidized metal such as chromium or titanium in two-layer deposition process. The total length, l_T, of an *E*-plane insert is represented as $l_T=l_M+2l_G$, with the edge parts of length l_G covered by graphene. Frequency tunability stems from the changes in boundary conditions at graphene stripes, as described in detail in [22].

As viewed from the angle of the normalized dominant mode equivalent circuit of the *E*-plane inserts [44], equivalent circuit reactances X_s and X_p become tunable as illustrated in the bottom left part of Fig. 1. As a consequence, the parameters of an equivalent impedance inverter (*K*-inverter) are affected. Primarily, the equivalent electrical length at ports due to the inserts, ϕ, becomes frequency tunable. As the equivalent circuit models of *E*-plane inserts exhibit nonlinear frequency dependence around the desired central frequency, and also due to the losses in graphene that are higher than in the purely metallic parts of the structure, accurate analysis mandates full-wave numerical electromagnetic computations of wave propagation. Also, equivalent circuit of a higher complexity could be used in the extraction of model parameters using the full-wave numerical EM computations or measurements. Here, the state-of-the-art commercial software package HFSS [45] is employed for the design space mapping and the subsequent filter design. Standard WR-2.2 waveguide section ($a=2b=559.0\,\mu$m) is assumed in the examples. Consistently with the examples from [22], quartz support thickness, *d*, is determined so as to satisfy $d/a=1/16$. The quartz dielectric constant and loss tangent are $\varepsilon_r = 3.78$ and $\tan\delta = 0.000228$, respectively. Skin effect in copper is modeled using the DC conductivity $\sigma_{Cu} = 58.0$ MS/m .

The surface conductivity of graphene, which depends on frequency as well as on the chemical potential, is incorporated into the HFSS by modeling a graphene sheet as an Impedance Boundary Condition surface. Expressions (3) and (4) have been used. Please note, that the L_g/R_g ratio depends only on the quality of graphene being used in a particular study; therefore, R_g was the externally input design parameter and the surface reactance, $X_g=\omega L_g$, was modeled as $X_g=f\pi\hbar R_g/(\Gamma q_e)$, in order to obtain the design space maps such as those shown in Fig. 3. Frequency coefficient, $C_f=f\pi\hbar/(\Gamma q_e)$, was input as a Design Dataset, where the values are tabulated versus frequency, and R_g was input using the tabulated data, corresponding to the linearly changing μ_c, for the Parametric Sweep. The filter design procedures were mainly using the bordering values of $\mu_c=0.2$ eV and $\mu_c=1.0$ eV; several other values of μ_c were also used to check the filtering responses. For these analyses, both R_g and X_g were input using the HFSS/ Design Datasets option, for a predefined set of μ_c values.

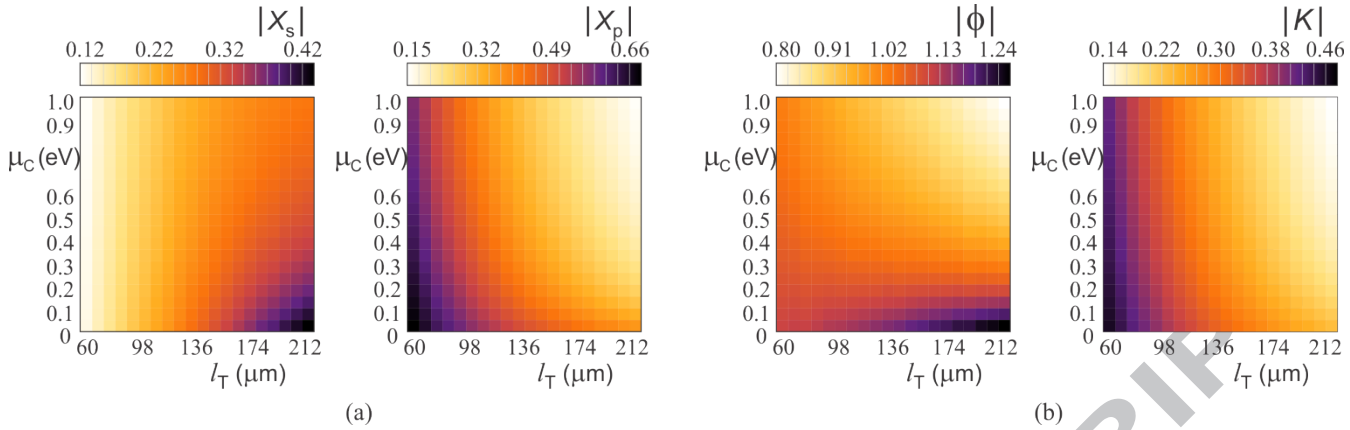

Fig. 3. Influence of the chemical potential, μ_c, on the normalized dominant mode equivalent circuit parameters, X_s, X_p, K, and ϕ, of a graphene resonator, for a range of E-plane insert lengths. The length of the graphene stripes covering the edges of an E-plane insert is taken as 25% of the insert length, i.e., the parameter l_G is varied from 15 μm to 53 μm with the total length equal to $l_T=4l_G$. Results are shown for the 400 GHz frequency. (a) Reactances $|X_s|$ and $|X_p|$. Material losses are moderate: $|\mathrm{Arg}(X_s)|<1.69°$, $|\mathrm{Arg}(X_p)|<2.75°$. It can be seen that X_s and X_p are significantly modified by μ_c. For very low μ_c, material losses are the highest; therefore, we use the $\mu_c\in[0.2\,\mathrm{eV},1.0\,\mathrm{eV}]$ interval to tune the surface conductivity, while keeping the desired function of the E-plane inserts. (b) Impedance inverter parameters, $|K|$ and $|\phi|$. $|\mathrm{Arg}(K)|<1.89°$, $|\mathrm{Arg}(\phi)-180°|<1.64°$. For $\mu_c\in[0.2\,\mathrm{eV},1.0\,\mathrm{eV}]$, parameter K ("gain") predominantly depends on the insert length. The equivalent electrical length at ports, ϕ, strongly depends on the material properties. Larger variation of ϕ is observed for larger insert lengths.

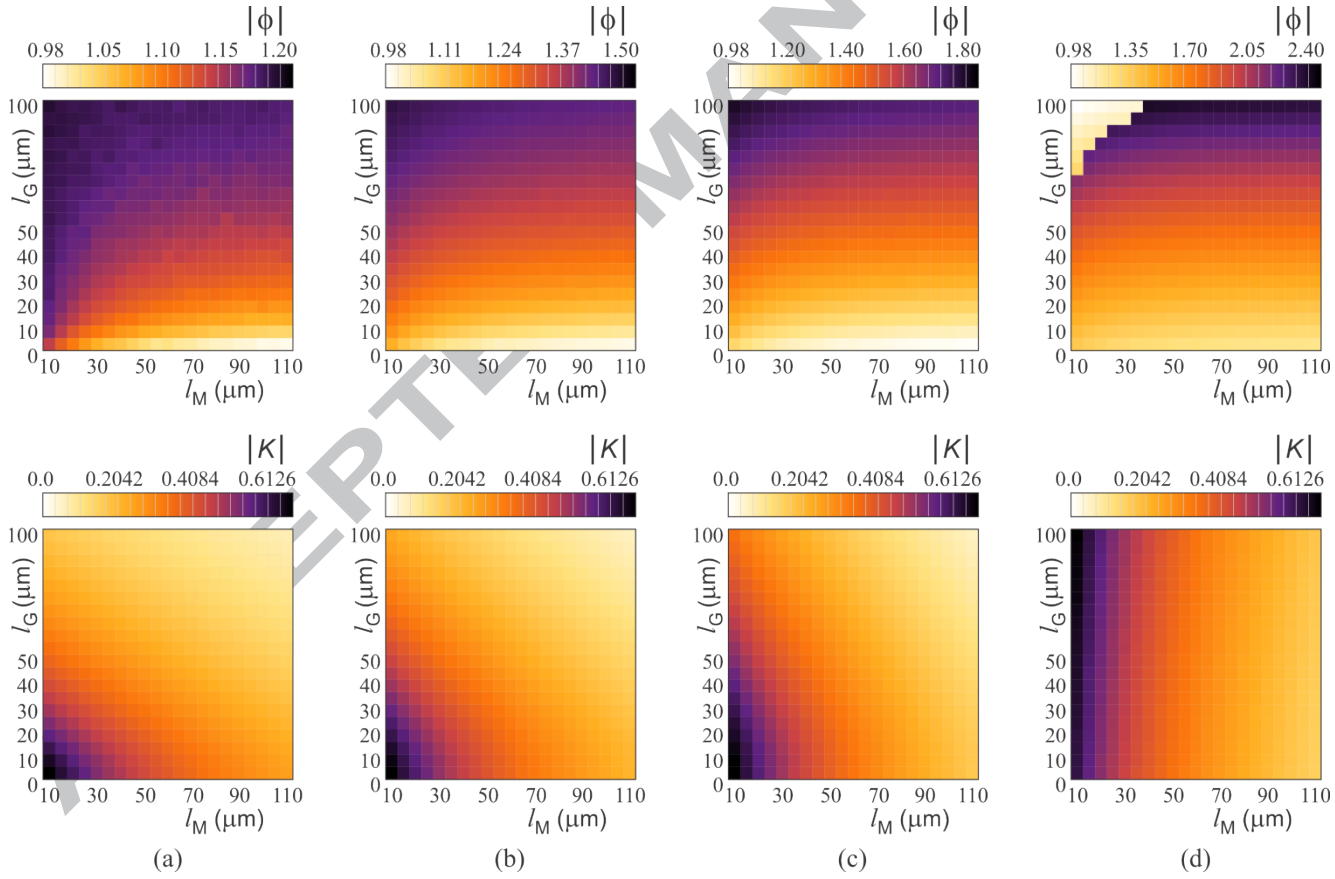

Fig. 4. Dependence of the impedance inverter parameters on the lengths of graphene and metallization for the combined graphene-metal E-plane inserts. Results are shown for the 400 GHz frequency, for the chemical potential (a) $\mu_c=1.00$ eV, (b) $\mu_c=0.40$ eV, (c) $\mu_c=0.20$ eV, (d) $\mu_c=0.05$ eV. Please note the differences in scales corresponding to the electrical length at ports, ϕ, necessary to present the dynamic range in each of the four cases. In case that $\mu_c=0.05$ eV, the K parameter almost entirely depends on the metallization length. In case that $\mu_c>0.20$ eV, each desired K value results in an (l_M, l_G) curve allowing for a choice of insert dimensions providing the required tunability, determined by the l_G, while fulfilling the requirement on the value of K. While the K parameter for a given (l_M, l_G) point varies slightly with μ_c, without significantly affecting the desired quality of the filtering characteristic, there is a pronounced variation of the ϕ parameter with μ_c that depends on the l_G. These features of carbon based inserts are essential in the design of graphene filters.

Initial analyses of the design space parameters have been performed with an aim to assess the system behavior for various configurations and to narrow the parameter intervals of interest for further design. Analyses included various sets of resonator dimensions (l_M, l_G), covering the frequency range 325–500 GHz, and chemical potential range [0 eV, 1 eV], so as to model the changes of the material properties. For each of the considered design space points, the scattering parameters corresponding to the waveguide discontinuity have been computed using the HFSS. The equivalent circuit reactances, X_s and X_p, normalized with respect to the waveguide charac-teristic impedance for the dominant mode, Z_C, were accurately determined from the knowledge of *S*-parameters [46]:

$$jX_s = \frac{1+S_{11}-S_{21}}{1-S_{11}+S_{21}}, \quad jX_p = \frac{2S_{21}}{(1-S_{11})^2 - S_{21}^2}. \qquad (5)$$

Subsequently, the parameters K and ϕ, used in the design of filters incorporating the *E*-plane inserts were obtained from

$$\tan(2\arctan K) = \frac{2X_p}{1+2X_pX_s+X_s^2}, \qquad (6)$$

$$\phi = -\arctan(2X_p + X_s) - \arctan(X_s). \qquad (7)$$

The results of these initial analyses are represented by the data shown in Fig. 3 and Fig. 4. The shown data correspond to the 400 GHz frequency, which is used in subsequent examples as the filter center frequency of the lowest band. Qualitative behavior of the carbon based *E*-plane inserts is similar at other frequencies. Figure 3 gives an insight into the influence of the chemical potential, μ_c, on the normalized dominant mode equivalent circuit parameters used in the filter design. For lossless filters, all four parameters are real. For the graphene filters, there are relatively small losses due to the dissipation in material, which can be treated as perturbation. Complex arguments are listed for the worst-case data points. Somewhat higher losses for $\mu_c \in [0.0\,\text{eV}, 0.2\,\text{eV}]$ impede desired functioning of the inserts; thus, the $\mu_c \in [0.2\,\text{eV}, 1.0\,\text{eV}]$ interval has been selected for resonant frequency tuning in [22] and here. We observe that the parameter K predominantly depends on a length of an insert, whereas the equivalent electrical length at ports, ϕ, strongly depends on the material properties. Figure 4 shows the impedance inverter parameters for different combinations of l_M and l_G, for four values of the chemical potential: μ_c=1.00 eV, μ_c=0.40 eV, μ_c=0.20 eV, μ_c=0.05 eV (Fig. 4(a), 4(b), 4(c), 4(d), respectively). Complex argument ranges are listed separately, in Table II. It is seen that the losses for μ_c=0.05 eV are too high. Additionally, there is almost no connection between l_G and the K parameter, which would result either in the very small values of l_G being used, or deterioration of filtering properties when μ_c is altered. We can see from Fig. 4, that it is optimal to choose such (l_M, l_G), which result in the sufficient change of electrical length, ϕ, to attain the required tunability and which also correspond to the K values obtained by the lowpass prototype design [46], [47].

TABLE II
FIGURES OF MERIT FOR THE LOSSES IN GRAPHENE (FOR THE FIG.4 DATA)

μ_c (eV)	1.00	0.40	0.20	0.05
$\lvert\text{Arg}(K)\rvert$	0.25–2.56	0.25–3.97	0.20–4.20	0.14–8.20
$\lvert\text{Arg}(\phi) - 180°\rvert$	0.30–1.43	0.30–2.09	0.30–2.23	0.30–4.75

3. Design procedure for carbon based filters

The design method that we deem the most efficient in the design of this type of filters relies on the computation of impedance inverter parameters utilizing the modern computer aided engineering (CAE) tools and the subsequent optimization and tuning to achieve the best results. The entire procedure will be illustrated by a design of an example filter. The center frequency of the lowest band has to be set first, as the material losses are the highest for the low chemical potential, i.e., μ_c=0.20 eV, and it is important to attain the adequate frequency response in this band. We set the lowest frequency of interest to f_0=400 GHz. Next, we set the target tunability at larger than 5%, i.e., at least 20 GHz. Also, a fractional bandwidth of about 5% should be easily attainable; however, the insertion loss needs to be at a reasonable level and the stop-band attenuation sufficient. We start from a fifth order Chebyshev lowpass prototype and require a flat passband response with the allowed ripple level of 0.01 dB. In this case, the lumped element lowpass prototype values are equal to $g_0 = g_6 = 1.0000$, $g_1 = g_5 = 0.7563$, $g_2 = g_4 = 1.3049$, $g_3 = 1.5773$. Due to the unavoidable losses with the carbon based filters, which are in tradeoff with the desired tunability, the obtained filter bandwidth is smaller than the one planned for lossless lowpass prototype. Therefore, the planned bandwidth should be taken wider than the desired one. In this case, the prototype bandwidth of 10%, $BW = 0.10$, shows quite sufficient. The normalized gains of the impedance inverters are determined as

$$k_1=\sqrt{\frac{\pi\cdot BW}{2g_0g_1}},\ k_i=\frac{\pi\cdot BW}{2\sqrt{g_{i-1}g_i}},\ i=2,\ldots,N-1,\quad k_N=\sqrt{\frac{\pi\cdot BW}{2g_{N-1}g_N}}. \tag{8}$$

The leftmost plot in Fig. 5 depicts the K values corresponding to the E-plane inserts at $f_0=400\,\text{GHz}$ for $\mu_c=0.20\,\text{eV}$. We need to choose the (l_M, l_G) dimensions for each of the six inserts in a fifth order bandpass filter (N–1=5), so that the K values equal k_i of given inserts, namely $k_1=k_6=0.456$, $k_2=k_5=0.158$, $k_3=k_4=0.109$. Please note, that the design space mapping was previously conducted for a wider range of dimensions (l_M, l_G), than that shown in Fig. 4, in order to cover all of the required k_i values. For the sufficient resolution in (l_M, l_G), either the aggressive design space mapping with small steps is done, or (which we recommend) a two-dimensional spline interpolation is used, based on computed data points. Similarly, the mapped K and ϕ data is required for a range of frequencies of interest. For the maximal desired tunability between 2.5% and 12.5%, we need the data for the 410–450 GHz range, for $\mu_c=1.00\,\text{eV}$. For example, Fig. 5 shows the K and ϕ data at $f_0=400\,\text{GHz}$ for $\mu_c=0.20\,\text{eV}$, as well as the ϕ data at 425 GHz for $\mu_c=1.00\,\text{eV}$.

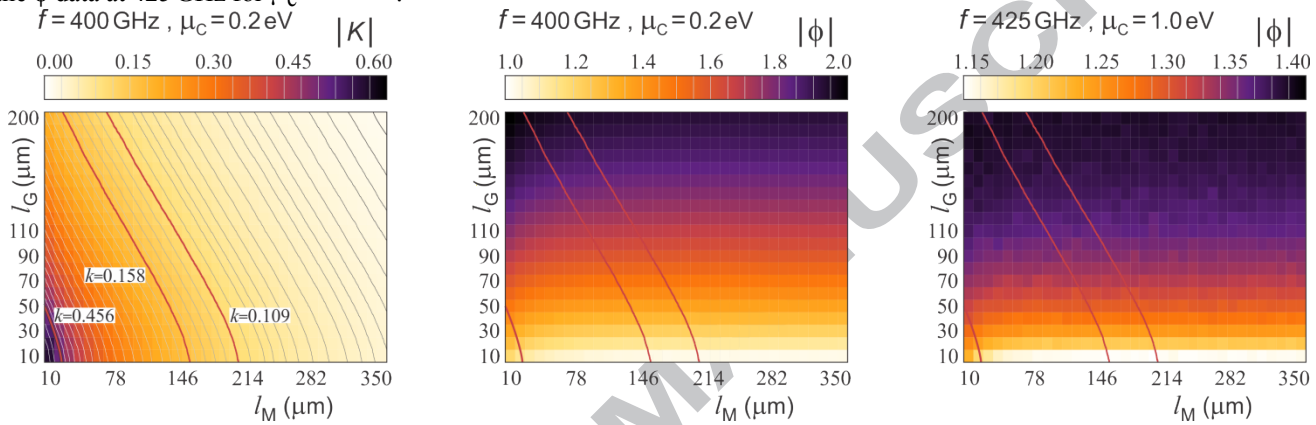

Fig. 5. Carbon based filter design utilizes extensive data sets obtained by the design space mapping for a number of (l_M, l_G) pairs, at a number of frequencies $f>f_0$, for $\mu_c=1.0\,\text{eV}$. The plot on the right shows an example of such data set for $f=425\,\text{GHz}$. The K and ϕ data are also required for the center frequency of the lowest band, f_0, for the lowest value of the chemical potential to be used, $\mu_c=0.2\,\text{eV}$, as shown in the leftmost and center plot, respectively. The geometrical loci of points in the data set shown on the left (red lines in all of the plots), where K equals k_i-s of the lowpass prototype filter (please see Eq.(8)), coincide with the allowed pairs (l_M, l_G) and also correspond to a specific variation of parameter ϕ with frequency. The latter can be alternatively represented as a dependence of frequency shift on the change in chemical potential; therefore, it is used to determine the right choice of (l_M, l_G), which can guarantee the desired maximal tunability range. It is not critical to initially consider the change of K with μ_c, as it varies mildly; however, it should be checked when (l_M, l_G) is obtained. If the desired filter response and other requirements, such as the tunable range and acceptable loss, cannot be simultaneously met, filter order should be increased, or passband ripple requirement somewhat relaxed, and the procedure repeated with a new set of k_i-s of the new lowpass prototype.

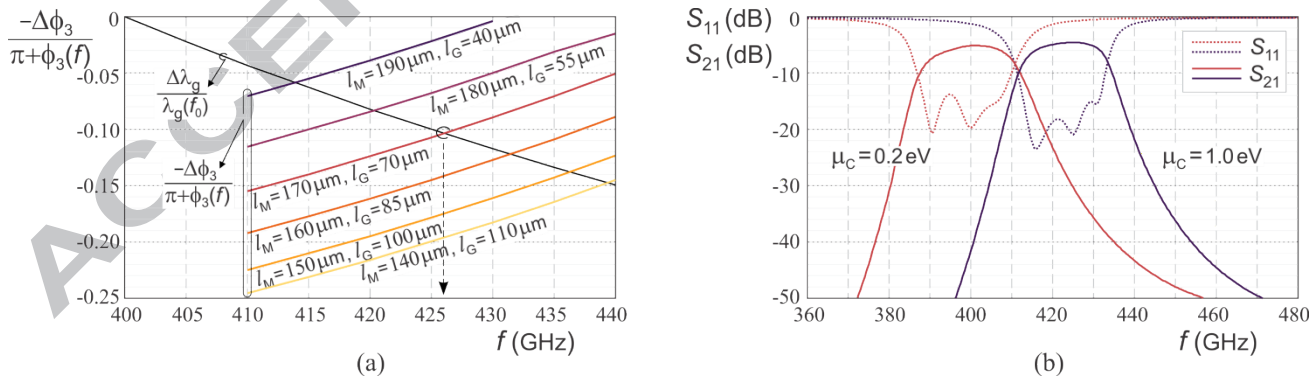

Fig. 6. Estimating tunable range and fine tuning of the specified filter response. Correspondence between the change in the electrical length at ports of an impedance inverter, $\Delta\phi$, and the guided wavelength, $\Delta\lambda_g$, is obtained based on the half-wave prototype method. It is given by (12) for the innermost resonator in the symmetrical structure of an odd order filter. (a) The right hand side of (12) has a known frequency dependence, while the left hand side of (12) depends on the choice of (l_M, l_G). Several curves are shown for some of the (l_M, l_G) pairs belonging to the loci of points (red lines) determined using the Fig. 5 data. Crossing points of these curves with the solid black line, which corresponds to the right hand side of (12), give tunable range estimates for each of the (l_M, l_G) pairs. The (l_M, l_G) pair is determined, that meets the specifications for maximal tunable range. (b) Due to the approximate nature of the half-wave prototype method, a full-wave numerical optimization in HFSS is used to match the lowest value of $\mu_c=0.2\,\text{eV}$ to exactly $f_0=400\,\text{GHz}$, as initially planned. We check that the maximal tunability equals or slightly exceeds the specified value, check on the achieved bandwidth and loss. If necessary, changes at the level of the lowpass prototype can be introduced to further improve the frequency response.

Previously prepared sets of the ϕ data, like the ones shown, covering the 410–450 GHz range are utilized to determine the appropriate (l_M, l_G) values to meet the tunability requirement. The procedure to determine the geometrical parameters is the following. The required k_i values correspond to the red lines in Fig. 5 (leftmost plot). These lines are also transferred to the two plots of the ϕ parameter in Fig. 5, for μ_c=0.2 eV at 400 GHz and μ_c=1.0 eV at 425 GHz. These are the geometrical loci of points (l_M, l_G) leading to the desired filtering response quality. For each point (l_M, l_G) on the red lines and each μ_c value, there is a different and unique variation of ϕ with frequency. Let us for a moment consider the innermost resonator of the fifth order filter. The equivalent electrical length at ports is equal for the two inserts adjacent to this resonator. If we denote this length as ϕ_3, $\phi_3<0$, and the guided wavelength as λ_g, according to the half-wave prototype design, the length of the innermost resonator is determined as

$$l_{rez3} = \frac{\lambda_g}{2}\frac{\pi+\frac{1}{2}\phi_3+\frac{1}{2}\phi_3}{\pi}. \qquad (9)$$

The guided wavelength, λ_g, is already calculated by the HFSS; it can be tabulated as an output and further used to determine the normalized variation of λ_g with frequency, with respect to the center frequency of the lowest band, f_0:

$$\frac{\Delta\lambda_g}{\lambda_g(f_0)} = \frac{\lambda_g(f)-\lambda_g(f_0)}{\lambda_g(f_0)}. \qquad (10)$$

The above normalized variation of λ_g with frequency, which is used in setting the desired tunability, is shown in Fig. 6(a) by a solid black line. The change in parameter ϕ, that follows the increase of the chemical potential from 0.2 eV to 1.0 eV, is also a function of (l_M, l_G). The physical lengths of resonators are fixed; therefore, the change in ϕ is compensated for by the resonant frequency shift towards the higher frequencies. The acceptable filtering response can be preserved only for certain combinations of the ϕ parameters of different *E*-plane inserts. Equating the physical length of the innermost resonator for μ_c=0.2 eV and μ_c=1.0 eV, we get

$$\frac{\pi+\phi_3(f_0,0.2\text{eV})}{\pi+\phi_3(f,1.0\text{eV})} = \frac{\lambda_g(f)}{\lambda_g(f_0)}, \qquad (11)$$

$$\frac{-\Delta\phi_3}{\pi+\phi_3(f,1.0\text{eV})} = \frac{\Delta\lambda_g}{\lambda_g(f_0)}. \qquad (12)$$

Please note that $\Delta\phi_3=\phi_3(f,1.0\text{eV})-\phi_3(f_0,0.2\text{eV})$ and also that the denominator on the left hand side uses the μ_c=1.0 eV data. The left hand side of (12) has been determined as a function of frequency f, for various points (l_M, l_G) on the loci of points corresponding to $k_3=k_4=0.109$. Several of these curves have been depicted in Fig. 6(a), which can be used to estimate and determine the tunability range. Namely, the solution of (12), for a given (l_M, l_G), corresponds to the crossing point of a given line with the black $\Delta\lambda_g/\lambda_g(f_0)$ line. The half-wave prototype method, particularly when the loss is non-negligible, is much less accurate than the full-wave computations. The tunability obtained by solving (12) is therefore considered an estimate. For our design example, the l_G=70 μm, l_M=170 μm combination of parameters was adopted, promising about 6.5% tunability and matching the $k_3=k_4=0.109$ requirement imposed for the two innermost inserts. Full-wave numerical electromagnetic modeling is subsequently used to check (i) the actual tunability range, as well as (ii) the insertion loss that should be expected from the medium-sized graphene stripes used in a fifth order low-ripple filter. With the (l_M, l_G) choice, the upper frequency estimate is set to f=426 GHz. We obtain an estimated l_{rez3}=262.04 μm, along with $\phi_3(f_0,0.2\text{eV})$=1.51, $\phi_3(f,1.0\text{eV})$=1.31. The next step is to determine ϕ_2, belonging to the loci of points (l_M, l_G) that provide $k_2=k_5=0.158$ for the second and fifth insert. Subsequently, ϕ_1 is determined on the (l_M, l_G) curve providing $k_1=k_6=0.456$ (outermost inserts). Conditions resulting in a good filter design are again derived from the half-wave prototype method, as

$$\frac{2\pi+\phi_3(f_0,0.2\text{eV})+\phi_2(f_0,0.2\text{eV})}{2\pi+\phi_3(f,1.0\text{eV})+\phi_2(f,1.0\text{eV})} \cong \frac{\lambda_g(f)}{\lambda_g(f_0)}, \qquad (13)$$

$$\frac{2\pi+\phi_2(f_0,0.2\text{eV})+\phi_1(f_0,0.2\text{eV})}{2\pi+\phi_2(f,1.0\text{eV})+\phi_1(f,1.0\text{eV})} \cong \frac{\lambda_g(f)}{\lambda_g(f_0)}. \qquad (14)$$

We adopted l_{G2}=70 μm, l_{M2}=120 μm, l_{G1}=30 μm, l_{M1}=20 μm, resulting in estimated l_{rez2}=261.55 μm, l_{rez1}=276.12 μm. As the outermost graphene stripes worsen the frequency response without contributing to the resonator lengths, these two stripes are omitted and l_{M1} is adjusted to l_{M1}=30 μm to account for the overall shortening. An HFSS model showed a slight shift from the planned f_0; therefore, the resonator lengths are fine tuned resulting in l_{rez3}=272 μm, l_{rez2}=272 μm, l_{rez1}=280 μm. The obtained filter characteristics are shown in Fig. 6(b), denoted by μ_c=0.2 eV. When the chemical potential is increased to μ_c=1.0 eV, a shift

of the filter center frequency from 400.0 GHz to 423.2 GHz is observed, i.e., a tunability of 5.8% is achieved. This is somewhat lower than theoretically predicted. Further adjustment of this maximal tunability can be iteratively performed, if desired. Varying the chemical potential from μ_c=0.2 eV to μ_c=1.0 eV, different frequency shifts are obtained, i.e., the continuous tunability. This is illustrated by the data shown in Table III. The filtering responses for the eight μ_c values given in Table III are also shown in the Fig. 1 (bottom right). Due to the changes in material surface conductivity, there is a very slight variation of the achieved fractional bandwidths, as can be seen from the data given in Table III. As for the second point of interest, the insertion loss for this fifth order filter is on the order of 5 dB. This is quite acceptable having in mind losses when single resonators are considered. This is also expected, since the electromagnetic field variations are more moderate for a row of inserts and resonators, than for a single resonator. The losses depend on the utilized amount of graphene; therefore, there is a trade-off with the required tunability range. Also, the losses are somewhat higher for the higher filter orders and better filtering responses. Thus, the proposed design procedure should be applied iteratively, including wider local region of the design space, in order to satisfy the imposed design specifications while keeping losses minimal. The proposed iterative adjustment of the low-pass prototype parameters and the physical structure of the filter could benefit from the circuit / full-wave co-simulation method, such as the one presented in [48]. It is particularly important to model the surface conductivity of graphene stripes using the impedance boundary conditions (same as in the HFSS), due to the almost negligible thickness of the graphene layers.

Finally, the design of asymmetrical *E*-plane inserts or even order filters, where the graphene stripe length of the central insert differs from the adjacent stripes belonging to the two inner resonators, is possible using the proposed method. It is necessary in such a case to compare a larger number of combinations of geometrical parameters and modify (12) to include two $\Delta\phi$-s, each one corresponding to a different set of (l_M, l_G) pairs. Instead of a crossing point shown in Fig. 6 (a), there would be a curve describing optimal (l_M, l_G) pairs.

TABLE III
THE CONTINUOUS TUNABILITY OBTAINED BY VARYING THE GRAPHENE CHEMICAL POTENTIAL IN THE RANGE $\mu_c \in [0.2\,\text{eV}, 1.0\,\text{eV}]$

μ_c (eV)	f_c (GHz)	*FBW*[a] (%)	*IL* (dB)
0.20	400.0	5.500	5.23
0.25	403.1	5.375	5.43
0.30	405.9	5.250	5.49
0.40	410.4	5.250	5.56
0.50	414.1	5.125	5.49
0.65	417.6	5.125	5.22
0.80	420.6	5.125	4.97
1.00	423.2	5.125	4.57

[a] *FBW* is calculated w.r.t. f_0 = 400 GHz in order to facilitate representation in GHz and mutual comparison of data

4. Conclusion

The design methodology for tunable sub-millimeter wave filters based on graphene has been proposed and explained in detail using an example of the fifth order filter. The analyzed filter design utilizes previously proposed graphene resonators, which have been thoroughly investigated for the frequency range 100 GHz–1100 GHz [22]. There is a trade-off between attaining the desired tunability for a single resonator and the insertion loss and quality factor [22]. Similar conclusion is drawn for the graphene filters, except that the problems are actually less pronounced in the filter design, due to the larger number of resonators that are combined to form a higher-order filter. Adjustment of the low-pass prototype parameters and the physical structure of the filter should be performed iteratively in order to achieve the most beneficial solution for the given specifications.

Acknowlegdements

This work was supported in part by the Serbian Ministry of Education, Science, and Technological Development under grants III-45003 and TR-32005.

References

[1] P. H. Siegel, "Terahertz technology," *IEEE Trans. Microw. Theory Techn.*, vol. 50, no. 3, pp. 910–928, Mar. 2002.
[2] S. S. Dhillon *et al.*, "The 2017 terahertz science and technology roadmap," *J. Phys. D: Appl. Phys.*, vol. 50, no 4, p. 043001, Jan. 2017.
[3] H. Koo, C. Kim, and S. Hong, "Design and analysis of 239 GHz CMOS push-push transformer-based VCO with high efficiency and wide tuning range," *IEEE Trans. Circuits Syst. I: Reg. Papers*, vol. 62, no. 7, pp. 1883–1893, Jul. 2015.
[4] P. Nayeri, M. Liang, R. A. Sabory-García, M. Tuo, F. Yang, M. Gehm, H. Xin, and A. Z. Elsherbeni, "3D printed dielectric reflectarrays: low-cost high-gain antennas at sub-millimeter waves," *IEEE Trans. Antennas Propagat.*, vol. 62, no. 4, pp. 2000–2008, Apr. 2014.
[5] Z. Xu, X. Dong, and J. Bornemann, "Design of a reconfigurable MIMO system for THz communications based on graphene antennas," *IEEE Trans. Terahertz Sci. Technol.*, vol. 4, no. 5, pp. 609–617, Sep. 2014.
[6] D. Correas-Serrano, J. S. Gomez-Diaz, A. Alù, A. Álvarez Melcón, "Electrically and magnetically biased graphene-based cylindrical wave-guides: analysis and applications as reconfigurable antennas," *IEEE Trans. Terahertz Sci. Technol.*, vol. 5, no. 6, pp. 951–960, Nov. 2015.
[7] P. L. Kirby, D. Pukala, H. Manohara, I. Mehdi, and J. Papapolymerou, "Characterization of micromachined silicon rectangular waveguide at 400 GHz," *IEEE Trans. Microw. Wirel. Compon. Lett.*, vol. 16, no. 6, pp. 366–368, Jun. 2006.

[8] K. M. K. H. Leong, W. R. Deal, V. Radisic, X. B. Mei, J. Uyeda, L. Samoska, A. Fung, T. Gaier, and R. Lai, "A 340–380 GHz integrated CB-CPW-to-waveguide transition for sub millimeter-wave MMIC packaging," *IEEE Trans. Microw. Wirel. Compon. Lett.*, vol. 19, no. 6, pp. 413–415, Jun. 2009.

[9] V. Sanphuang, N. Ghalichechian, N. K. Nahar, and J. L. Volakis, "Recon-figurable THz filters using phase-change material and integrated heater," *IEEE Trans. Terahertz Sci. Tech.*, vol. 6, no. 4, pp. 583–591, Jul. 2016.

[10] X. L. Guo, C. Xu, G. A. Zhang, Z. J. Zhang, H. H. Yin, and Z. L. Wang, "Tunable low-pass MEMS filter using defected ground structures (DGS) ," *Solid-State Electron.*, vol. 94, pp. 28–31, Apr. 2014.

[11] S. Jenabi, A. Malekabadi, D. Deslandes, F. Boone, and S. A. Charlebois, "Submillimeter wave GaAs Schottky diode application based study and optimization for 0.1–1.5 THz," *Solid-State Electron.*, vol. 134, pp. 65–73, Aug. 2017.

[12] T. Kawasaki, K. Sugawara, A. Dobroiu, T. Eto, Y. Kurita, K. Kojima, Y. Yabe, H. Sugiyama, T. Watanabe, T. Suemitsu, V. Ryzhii, K. Iwatsuki, Y. Fukada, J.-I. Kani, J. Terada, N. Yoshimoto, K. Kawahara, H. Ago, and T. Otsuji, "Graphene-channel FETs for photonic frequency double-mixing conversion over the sub-THz band," *Solid-State Electron.*, vol. 103, pp. 216–221, Jan. 2015.

[13] L. Sang, Y. Xu, Y. Wu, and R. Chen, "Device and compact circuit-level modeling of graphene field-effect transistors for RF and microwave applications," *IEEE Trans. Circuits Syst. I: Reg. Papers*, vol. 65, no. 8, pp. 2559–2570, Aug. 2018.

[14] B. Sensale-Rodriguez, R. Yan, M. M. Kelly, T. Fang, K. Tahy, W. S. Hwang, D. Jena, L. Liu, and H. G. Xing, "Broadband graphene terahertz modulators enabled by intraband transitions," *Nat. Commun.*, vol. 3, p. 780, Apr. 2012.

[15] R. Amin, C. Suer, Z. Ma, I. Sarpkaya, J. B. Khurgin, R. Agarwal, and V. J. Sorger, "A deterministic guide for material and mode dependence of on-chip electro-optic modulator performance," *Solid-State Electron.*, vol. 136, pp. 92–101, Oct. 2017.

[16] A. Tredicucci and M. S. Vitiello, "Device concepts for graphene-based terahertz photonics," *IEEE J. Sel. Top. Quantum Electron.*, vol. 20, no. 1, p. 8500109, Jan. 2014.

[17] C. Lim, A. Nirmalathas, M. Bakaul, P. Gamage, K.-L. Lee, Y. Yang, D. Novak, and R. Waterhouse, "Fiber-wireless networks and subsystem technologies," *J. Lightwave Technol.*, vol. 28(4), pp. 390-405, Feb. 2010.

[18] X. Yu, S. Jia, H. Hu, M. Galili, T. Morioka, P. U. Jepsen, L. K. Oxenløwe, "160 Gbit/s photonics wireless transmission in the 300-500 GHz band," *APL Photonics*, vol. 1, no. 8, p. 081301, Nov. 2016.

[19] S. W. Wong, K. Wang, Z. Chen, and Q. Chu, "Design of millimeter-wave bandpass filter using electric coupling of substrate integrated waveguide (SIW)," *IEEE Microw. Wirel. Comp. Lett.*, vol. 24, pp. 26–28, Jan. 2014.

[20] B. K. Kuanr, I. R. Harward, R. T. Deiotte, R. E. Camley, and Z. Celinski, "Magnetically tunable micro-strip band-stop filter: design optimization and characterization," *J. Appl. Phys.*, vol. 97, no. 10, p. 10Q103, May 2005.

[21] S. H. Lee, H.-D. Kim, H. J. Choi, B. Kang, Y. R. Cho, and B. Min, "Broadband modulation of terahertz waves with non-resonant graphene meta-devices," *IEEE Trans. Terahertz Sci. Technol.*, vol. 3, no. 6, pp. 764–771, Nov. 2013.

[22] A. Ž. Ilić, B. Bukvić, M. M. Ilić, and D. Budimir, "Graphene-based waveguide resonators for submillimeter-wave applications," *J. Phys. D: Appl. Phys.*, vol. 49, no. 32, p. 325105, Jul. 2016.

[23] Y. Guo, T. Zhang, W.-Y. Yin, and X.-H. Wang, "Improved hybrid FDTD method for studying tunable graphene frequency-selective surfaces (GFSS) for THz-wave applications," *IEEE Trans. Terahertz Sci. Technol.*, vol. 5, no. 3, pp. 358–367, May. 2015.

[24] T. Otsuji, S.A. Boubanga Tombet, A. Satou, H. Fukidome, M. Suemitsu, E. Sano, V. Popov, M. Ryzhii, and V. Ryzhii, "Graphene-based devices in terahertz science and technology," *J. Phys. D: Appl. Phys.*, vol. 45, no. 30, p. 303001, Jul. 2012.

[25] S. Luo, J. Yang, X. Song, X. Zhou, L. Yu, T. Sun, C. Yu, D. Huang, C. Du, and D. Wei, "Tunable-sensitivity flexible pressure sensor based on graphene transparent electrode," *Solid-State Electron.*, vol. 145, pp. 29–33, Jul. 2018.

[26] J. Heidler, S. Yang, X. Feng, K. Müllen, and K. Asadi, "Ferroelectric field-effect transistors based on solution-processed electrochemically exfoliated graphene," *Solid-State Electron.*, vol. 144, pp. 90–94, Jun. 2018.

[27] B. K. Sharma and J.-H. Ahn, "Graphene based field effect transistors: Efforts made towards flexible electronics," *Solid-State Electron.*, vol. 89, pp. 177–188, Nov. 2013.

[28] P. Kopyt, B. Salski, P. Zagrajek, D. Janczak, M. Sloma, M. Jakubowska, M. Olszewska-Placha, and W. Gwarek, "Electric properties of graphene-based conductive layers from DC up to terahertz range," *IEEE Trans. Terahertz Sci. Tech.*, vol. 6, no. 3, pp. 480–490, May. 2016.

[29] S. H. M. Jafri *et al.*, "Conductivity engineering of graphene by defect formation," *J. Phys. D: Appl. Phys.*, vol. 43, no. 4, p. 045404, Jan. 2010.

[30] S. Gulkis, M. Frerking, J. Crovisier, *et al.*, "MIRO: Microwave instrument for Rosetta orbiter," *Space Sci. Rev.*, vol. 128, no. 4, pp. 561–597, Feb. 2007.

[31] M.-T. Chen, C.-T. Li, Y.-J. Hwang, *et al.*, "AMiBA: Broadband heterodyne cosmic microwave background interferometry," *Astrophys. J.*, vol. 694, no. 2, pp. 1664–1669, Apr. 2009.

[32] K. Batrakov, P. Kuzhir, S. Maksimenko, N. Volynets, S. Voronovich, A. Paddubskaya, G. Valusis, T. Kaplas, Yu. Svirko, and Ph. Lambin, "Enhanced microwave-to-terahertz absorption in graphene," *Appl. Phys. Lett.*, vol. 108, no. 12, p. 123101, Mar. 2016.

[33] P. P. Kuzhir, A. G. Paddubskaya, N. I. Volynets, K. G. Batrakov, T. Kaplas, P. Lamberti, R. Kotsilkova, Ph. Lambin, "Main principles of passive devices based on graphene and carbon films in microwave–THz frequency range," *J. Nanophoton.*, vol. 11, no. 3, p. 032504, Sep. 2017.

[34] R. Kubo, "Statistical-mechanical theory of irreversible processes. I. General theory and simple applications to magnetic and conduction problems," *J. Phys. Soc. Jpn.*, vol. 12, no. 6, pp. 570–586, Jun. 1957.

[35] G. W. Hanson, "Dyadic Green's functions for an anisotropic, non-local model of biased graphene," *IEEE Trans. Antennas Prop.*, vol. 56, no. 3, pp. 747–757, Mar. 2008.

[36] G. W. Hanson, "Dyadic Green's functions and guided surface waves for a surface conductivity model of graphene," *J. Appl. Phys.*, vol. 103, no. 6, p. 064302, Mar. 2008.

[37] G. Lovat, "Equivalent circuit for electromagnetic interaction and transmission through graphene sheets," *IEEE Trans. Electromagn. Compat.*, vol. 54, no. 1, pp. 101–109, Feb. 2012.

[38] M. Orlita, C. Faugeras, P. Plochocka, P. Neugebauer, G. Martinez, D. K. Maude, A.-L. Barra, M. Sprinkle, C. Berger, W. A. de Heer, M. Potemski, "Approaching the Dirac point in high-mobility multilayer epitaxial graphene," *Phys. Rev. Lett.*, vol. 101, no. 26, p. 267601, Dec 2008.

[39] J. S. Gomez-Diaz, C. Moldovan, S. Capdevila, J. Romeu, L. S. Bernard, A. Magrez, A. M. Ionescu, and J. Perruisseau-Carrier, "Self-biased reconfigurable graphene stacks for terahertz plasmonics," *Nature Commun.*, vol. 6, p. 6334, Mar. 2015.

[40] M. Liu, X. Yin, and X. Zhang, "Double-layer graphene optical modulator," *Nano Lett.*, vol. 12, no. 3, pp. 1482–1485, Feb. 2012.

[41] M. Lobet, N. Reckinger, L. Henrard, and Ph. Lambin, "Robust electromagnetic absorption by graphene/polymer heterostructures," *Nanotechnology*, vol. 26, no. 28, p. 285702, Jun. 2015.

[42] P. P. Kuzhir, A. G. Paddubskaya, N. I. Volynets, K. G. Batrakov, S. A. Maksimenko, E. N. Golubeva, G. Valusis, T. Kaplas, N. Reckinger, M. Lobet, Ph. Lambin, "Effect of graphene grains size on the microwave electromagnetic shielding effectiveness of graphene/polymer multilayers," *J. Nanophoton.*, vol. 11, no. 3, p. 032511, Sep. 2017.

[43] M. Lobet, B. Majerus, L. Henrard, and Ph. Lambin, "Perfect electromagnetic absorption using graphene and epsilon-near-zero metamaterials," *Phys. Rev. B*, vol. 93, no. 23, p. 235424, Jun. 2016.

[44] Y. Konishi and K. Uenakada, "The design of a bandpass filter with inductive strip – planar circuit mounted in waveguide," *IEEE Trans. Microw. Theory Techn.*, vol. 22, pp. 869–873, Oct. 1974.

[45] ANSYS HFSS. Available: http://www.ansys.com
[46] R. J. Cameron, C. M. Kudsia, R. Mansour, "Design and physical realization of coupled resonator filters," in *Microwave Filters for Communication Systems*, 1st ed., Hoboken, NJ, USA: John Wiley & Sons, Inc, 2007.
[47] D. Budimir, *Generalized Filter Design by Computer Optimization*, 1st ed., Norwood, MA, USA: Artech House, Inc., 1998.
[48] M. Feliziani, S. Cruciani, and F. Maradei, "Circuit-oriented FEM modeling of finite extension graphene sheet by impedance network boundary conditions (INBCs)," *IEEE Trans. Terahertz Sci. Technol.*, vol. 4, no. 6, pp. 734–740, Nov. 2014.

Andjelija Ž. Ilić received the Dipl. Ing., M.Sc., and Ph.D. degrees in electrical engineering from the University of Belgrade, Serbia, University of Massachusetts Dartmouth, Dartmouth, MA, USA, and University of Belgrade, Serbia in 1998, 2004, and 2010.

She is currently an Assistant Professor with the Institute of Physics Belgrade. She was a Postdoctoral Research Associate with the University of Westminster, London, U.K., during 2013–2014. Her research interests are in applied and computational electromagnetics.

Dr. Ilić was the recipient of the 2006 Young Scientist and the 2014 Best Paper ETRAN Awards, as well as the "Prof. Aleksandar Marinčić" Award given annually by the IEEE MTTS Serbia chapter, for the best journal paper in 2016.

Branko M. Bukvić received the Dipl. Ing., M.Sc., and Ph.D degrees in electrical engineering from the University of Belgrade, Belgrade, Serbia, in 2009, 2011, and 2017, respectively. During the PhD studies he spent two years at the University of Westminster, London, UK.
His research interests are in the development and design of high power RF amplifiers, design and modeling of microwave circuits and devices, and carbon-based microwave components and circuits.

Dr. Bukvić was the recipient of the prestigious Award "Prof. Aleksandar Marinčić" given annually by the IEEE MTTS Serbia chapter, for the best journal paper in 2016.

Djuradj Budimir received the Dipl. Ing. and M.Sc. degrees in electronic engineering from the University of Belgrade, Belgrade, Serbia, and the Ph.D. degree in electronic and electrical engineering from the University of Leeds, Leeds, U.K.
In March 1994, he joined the Kings College London, University of London. Since January 1997, he has been with the Faculty of Science and Technology, University of Westminster, London, UK. He is a Reader of wireless communications and leads the Wireless Communications Research Group. His expertise includes design of circuits from RF through microwave to millimetre-wave frequencies for 4G and 5G communications. He has won awards for his journal papers. Dr. Budimir is a Member of the EPSRC Peer Review College and a Charter Engineer.

Milan M. Ilić received the Dipl. Ing. and M.Sc. degrees in electrical engineering from the University of Belgrade, Serbia, and the Ph.D. degree from the University of Massachusetts Dartmouth, Dartmouth, MA, USA, in 2003.
He is a Professor with the School of Electrical Engineering, University of Belgrade and Affiliated Faculty Member with the ECE Department, Colorado State University. His research interests include computational electromagnetics, applied electromagnetics, antennas, and active and passive microwave components and circuits.

Dr. Ilić was the recipient of the 2005 IEEE Microwave Theory and Techniques Society (IEEE MTT-S) Microwave Prize. He was the recipient of the 2016 "Prof. Aleksandar Marinčić" Award, given annually by the IEEE MTTS Serbia.

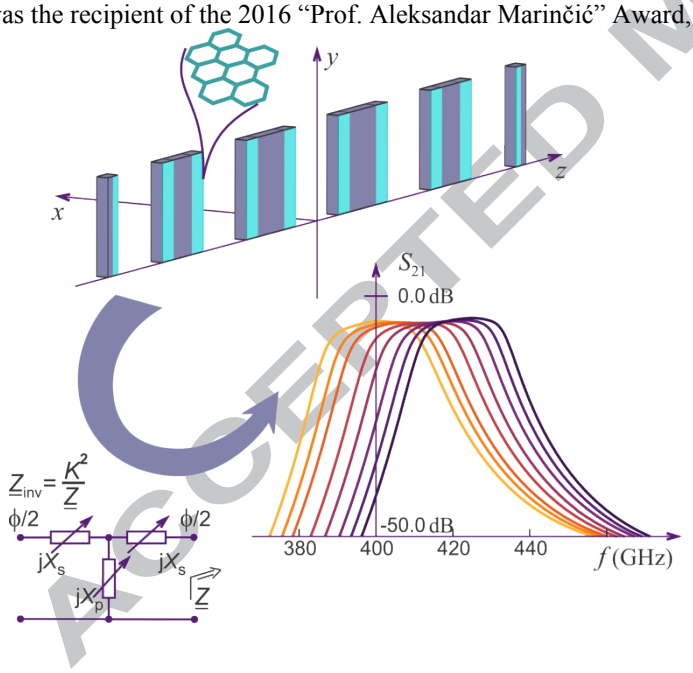

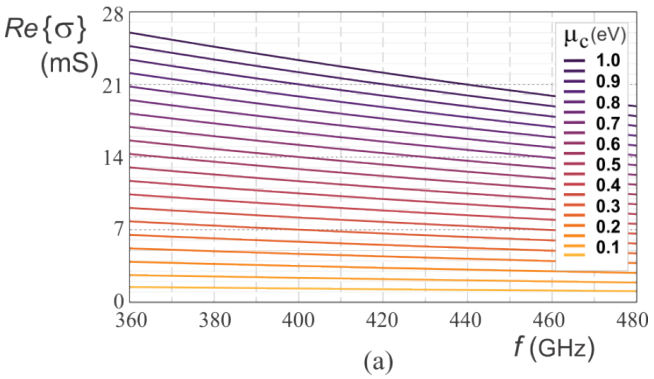

(a)

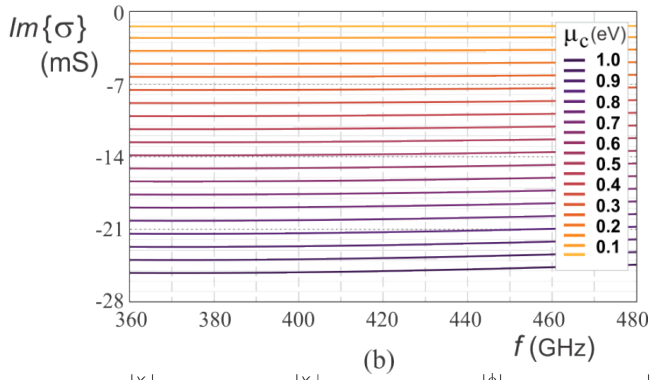

(b)

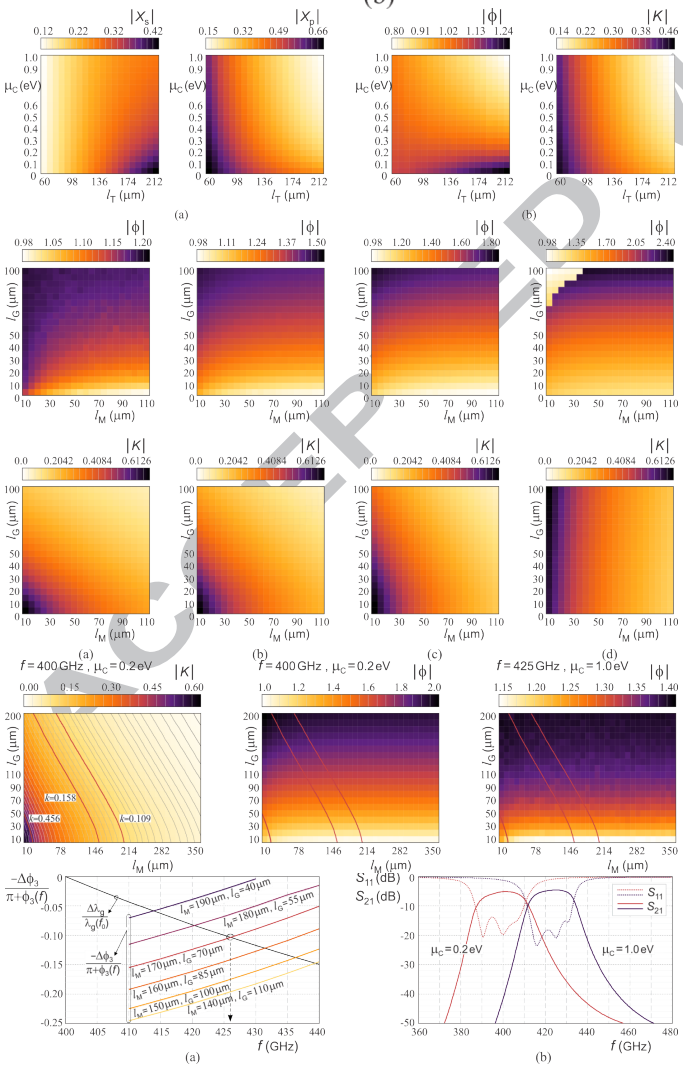

Manuscript title:

Design methodology for graphene tunable filters at the sub-millimeter-wave frequencies

Authors:

Andjelija Ž. Ilić[a,*], Branko M. Bukvić[b], Djuradj Budimir[c,d], and Milan M. Ilić[d,e]

(Family names: Ilić, Bukvić, Budimir, Ilić)

(Email addresses: andjelijailic@ieee.org, bukvic.branko@gmail.com, d.budimir@westminster.ac.uk, milanilic@etf.bg.ac.rs)

Highlights

- Detailed design space mapping for the combined graphene-metal waveguide resonators
- Design method to systematically achieve the specified tunable filtering response
- State-of-the-art full-wave numerical EM simulations and model parameter extraction
- Design curves for the combined graphene-metal filter tunability adjustment
- Fifth-order Chebyshev filter example and explanation of design trade-offs

Andjelija Ž. Ilić received the Dipl. Ing., M.Sc., and Ph.D. degrees in electrical engineering from the University of Belgrade, Serbia, University of Massachusetts Dartmouth, Dartmouth, MA, USA, and University of Belgrade, Serbia in 1998, 2004, and 2010.

She is currently an Assistant Research Professor with the Institute of Physics Belgrade. She was a Postdoctoral Research Associate with the University of Westminster, London, U.K., during 2013–2014. Her research interests are in applied and computational electromagnetics.

Dr. Ilić was the recipient of the 2006 Young Scientist and the 2014 Best Paper ETRAN Awards, as well as the "Prof. Aleksandar Marinčić" Award given annually by the IEEE MTTS Serbia chapter, for the best journal paper in 2016.

Branko M. Bukvić received the Dipl. Ing., M.Sc., and Ph.D degrees in electrical engineering from the University of Belgrade, Belgrade, Serbia, in 2009, 2011, and 2017, respectively. During the PhD studies he spent two years at the University of Westminster, London, UK.

He is currently an Assistant Research Professor employed by the IMTEL Communications a.d., Belgrade, Serbia. His research interests are in the development and design of high power RF amplifiers, design and modeling of microwave circuits and devices, and carbon-based microwave components and circuits.

Dr. Bukvić was the recipient of the prestigious Award "Prof. Aleksandar Marinčić" given annually by the IEEE MTTS Serbia chapter, for the best journal paper in 2016.

Djuradj Budimir received the Dipl. Ing. and M.Sc. degrees in electronic engineering from the University of Belgrade, Belgrade, Serbia, and the Ph.D. degree in electronic and electrical engineering from the University of Leeds, Leeds, U.K.

In March 1994, he joined the Kings College London, University of London. Since January 1997, he has been with the Faculty of Science and Technology, University of Westminster, London, UK. He is a Reader of wireless communications and leads the Wireless Communications Research Group. His expertise includes design of circuits from RF through microwave to millimetre-wave frequencies for 4G and 5G communications. He has won awards for his journal papers. Dr. Budimir is a Member of the EPSRC Peer Review College and a Charter Engineer.

Milan M. Ilić received the Dipl. Ing. and M.Sc. degrees in electrical engineering from the University of Belgrade, Serbia, and the Ph.D. degree from the University of Massachusetts Dartmouth, Dartmouth, MA, USA, in 2003.

He is a Professor with the School of Electrical Engineering, University of Belgrade and Affiliated Faculty Member with the ECE Department, Colorado State University. His research interests include computational electromagnetics, applied electromagnetics, antennas, and active and passive microwave components and circuits.

Dr. Ilić was the recipient of the 2005 IEEE Microwave Theory and Techniques Society (IEEE MTT-S) Microwave Prize. He was the recipient of the 2016 “Prof. Aleksandar Marinčić” Award, given annually by the IEEE MTTS Serbia.